*Tellus* (1989), *41A*, 416–435

# Fractal drifter trajectories in the Kuroshio extension

By A. R. OSBORNE, *Istituto di Cosmogeofisica del C.N.R., Corso Fiume 4, Torino 10133, Italy,*
A. D. KIRWAN, JR., *Department of Oceanography, Old Dominion University, Norfolk, VA 23508, USA,*
A. PROVENZALE, *Istituto di Cosmogeofisica del C.N.R., Corso Fiume 4, Torino 10133, Italy*
and L. BERGAMASCO, *Istituto di Fisica Generale dell'Università, Corso M. D'Azeglio 46, Torino 10125, Italy*

(Manuscript received 27 June 1988; in final form 2 February 1989)

ABSTRACT

We study the fractal and scaling properties of the Lagrangian trajectories of three satellite-tracked, freely drifting buoys (drifters) placed in the Kuroshio extension region during 1977. Over a period of about one year, the drifters, whose positions followed approximately the motions of fluid parcels in the near-surface layer, traveled almost the entire width of the Pacific Ocean. During this time, the drifters followed what may be described as highly erratic paths, while on the average being advected eastward in the zonal flow. Here we apply four different data analysis methods, based on the mathematics of fractals, to the drifter paths. We find that for space scales extending from at least 20 to 150 km and time scales from 1.5 days to 1 week, each of the trajectories displays fractal and scaling behavior with a fractal dimension of approximately 1.3. The multifractal nature of the drifter trajectories is also explored. The implication of these results is that the near-surface Lagrangian mesoscale motions in the Kuroshio Extension exhibit fractal properties in a range of scales normally attributed to geophysical fluid dynamical turbulence. These results evidently provide the first experimental evidence that fluid parcel trajectories in large-scale ocean flows can exhibit fractal behavior. A relation between the observed value of the fractal dimension and the properties of the power spectrum of a typical drifter position coordinate is also exploited. We finally discuss some of the possible physical implications of these results for the study of geophysical fluid dynamical flows.

## 1. Introduction

The use of freely drifting, satellite-tracked surface buoys (drifters) and of deep subsurface SOFAR floats is a relatively recent development in the experimental study of large- and mesoscale ocean dynamics. These novel measurement techniques, which are crucially dependent upon remote-sensing technologies, have the capability of providing a large amount of information on the general circulation and on its variability. The trajectories of the drifters and of the floats represent a (quasi) Lagrangian description of the fluid flows since the free buoys may be considered to approximately follow the individual parcels of fluid in their motions throughout the ocean. While scarcely useful in tracking vertical and convective motions, the drifter measurements are obviously best employed in determining some of the properties of large-scale, essentially two-dimensional, geophysical flows.

To quantitatively interpret the observations now available from several ocean regions, various approaches and time series analysis methods have been considered by different authors. Since large-scale motions may possess an energetic turbulent component, the drifter paths may be highly irregular and statistical approaches must consequently be employed. The techniques most commonly adopted may be grossly subdivided into two main categories, depending upon the scope of the analysis. The first approach is essentially based on considering the "ensemble" behavior of many trajectories, with the aim of

reconstructing the overall characteristics of the circulation. Some examples of these kinds of analyses are provided by Kirwan et al. (1978), McNally et al. (1983) and McNally and White (1985), who studied the circulation in the North Pacific; by Richardson (1983), who studied the mean kinetic energy distribution in the North Atlantic; by Molinari et al. (1981), who analyzed the surface currents in the Caribbean Sea, by Schmitz et al. (1981), Owens (1984), and Shaw and Rossby (1984), whose work was devoted to the study of the Gulf Stream and of the subtropical gyre with SOFAR floats; by Royer and Emery (1984), who studied the circulation in the Bering Sea, by Hofmann (1985), who analyzed the circulation in the Southern Ocean; and by Peterson (1985), who compared drifter data and current-meter measurements at Drake passage in the Southern Ocean. An extensive review of the drifter approach and of the technical problems related to the use of satellite-tracked drifters may be found in Kirwan and Cresswell (1982).

The second approach to the analysis of drifter data is in a sense complementary to the former and it is based on considering the statistical properties of the motions of individual drifters (single-particle diffusion) or on two-parcel separation studies. In this context, Davis (1982, 1983) has provided a theoretical basis for analyzing single-parcel and two-particle statistics and for relating Eulerian and Lagrangian statistical properties. These studies represent an extension of classic approaches to Lagrangian diffusion in three dimensional, homogeneous and isotropic turbulence to geophysical fluid dynamical flows. The papers by Davis (1985) on the experimental program CODE and by Fahrbach et al. (1986) on the Atlantic Equatorial Undercurrent are recent examples of parcel separation studies in ocean flows.

In the present analysis, we consider a different approach and focus on the individual geometrical properties of three drifter trajectories in the Kuroshio extension region, a part of the Pacific Ocean known for its intense mesoscale variability. Although the drifter paths are quite irregular and apparently strongly different from each other, we show that there are some fundamental geometrical and statistical properties which are common to all trajectories. In particular we consider the fractal and scaling behavior of the drifter motions and discuss how the fractal properties of the fluid parcel trajectories may be related to the dynamical motion. The study of the fractal properties of fully developed turbulent flows was stimulated over 15 years ago by the work of Mandelbrot (1972, 1974, 1975), who suggested for the first time that a full understanding of turbulent fluid flows requires consideration of the scaling and fractal properties of the motion. Here we concentrate on an unexplored aspect of the relationship between turbulence and fractals and provide original experimental evidence that fluid parcel trajectories in a large-scale ocean flow may be viewed as fractal curves with a fractal dimension of approximately 1.3. This research is a continuation of a previous study (Osborne et al., 1986), in which we considered the possibility that these Lagrangian observations of the dynamics in the Kuroshio extension could be interpreted in terms of deterministic chaos (for an introduction to deterministic chaos and related topics see, e.g., Eckmann and Ruelle, 1985). That analysis provided no evidence for low-dimensional chaos, but instead indicated that the drifter trajectories in the ocean surface layer displayed many of the characteristics of fractal curves. This paper is thus devoted to the systematic study of these fractal properties.

The approach taken here differs in at least 3 ways from other experimental studies on fractal properties of turbulent flows. First the analysis relies on Lagrangian data; hence we focus on the fractal nature of fluid parcel trajectories. We are not aware of any other experiments which have utilized particle trajectories to estimate fractal properties. A second important difference is that the data analyzed here come from a geophysical fluid dynamical (GFD) system whose dynamics are known to be significantly different from three-dimensional dynamics. Finally we stress that the data studied here come from a natural, large-scale system and not from a controlled laboratory experiment.

The use of Lagrangian data is particularly appropriate in the study of fractal behavior in that Lagrangian trajectories are amenable to at least four types of fractal analyses. Three of these techniques are devoted to the study of the so-called monofractal properties of the drifter trajectories. Of these the "yardstick" length and

the correlation dimension method provide information on spatial scales over which fractal and scaling properties hold. The third method, based on the calculation of the scaling exponent, gives comparable time scale information. Thus, the fractal analysis of Lagrangian data has the potential to give both time and space-scale information. The fourth method which we employ is based on the use of a box counting algorithm and is devoted to the study of the multifractal nature of the drifter data. This method also provides space-scale information.

Because of these attributes the data herein considered can also be used to address several basic issues in the fractal analysis of experimental signals. First, 3 separate trajectories are analyzed. This is important since, with just a single signal, there is concern that some unsuspected bias may distort the results. By contrast we have 6 signals available for fractal analysis; thus by combining signals in different ways we are able to test the internal consistency of the analyses. Second, since we use several different fractal analysis methodologies, we are able to address the important question of whether different methods of calculating the fractal dimension give comparable results when applied to experimental data. Finally, we also exploit a suggestion by Mandelbrot (1977, 1982), together with an extension of a result of Panchev (1971), to estimate the logarithmic slope of the (displacement) power spectrum in the fractal scaling range from the measured values of the fractal dimension of the drifter trajectories.

The remainder of this paper is organized as follows. Section 2 gives a brief description of the experiment and of the data considered herein. Section 3 summarizes the aspects of fractal behavior for curves on a plane that are pertinent to this study. In particular, we review the notions of scaling exponents, yardstick length and the correlation function as methods for determining the fractal dimension of data. We also discuss how the fractal dimensions can be used to infer the slope of the displacement power spectrum in the case of simple (or "mono") fractals and we introduce the concepts of multifractality and multiple scaling. In Section 4, these methodologies are applied to the data described in Section 2. The statistical uncertainties encountered in this analysis are discussed in Section 5, and some of the possible physical implications of the results found in the present research are discussed in Section 6.

## 2. Description of data

The data analyzed here consists of the trajectories of 3 drifters deployed in the Kuroshio current off the coast of Japan in 1977. These data were included in the synthesis of the North Pacific subtropical circulation compiled by McNally et al. (1983). Part of the data used here were also analyzed by Vastano et al. (1985) and Kirwan and Cresswell (1982). The classical oceanographic interpretation of these data has thus been well established. Further information on the descriptive and statistical oceanographical aspects of the drifter trajectories can be found in the referenced papers.

The drifters were drogued by parachutes to a depth of 100 m. This large drogue depth was chosen to minimize spurious wind and wave-drift effects on the buoy motions; the trajectories are thought to be representative of fluid particle paths in large scale ocean flows. The problem of closely relating the drifter motions to the real fluid particle trajectories is a difficult and debated issue. In a study of drifter motions in the North Pacific Ocean, for example, McNally (1981) reported the puzzling observation that both drogued and undrogued drifters behaved similarly, both being very sensitive to the local winds. This result was however obtained for drifters with a drogue depth of only about 30 m, and is thus relevant to drifters which measure the dynamics in the surface mixed layer and which are strongly influenced by the local atmospheric (and wave) forcing. Drifters with a much larger drogue depth are by contrast thought to behave differently, following more closely the large and mesoscale flows below the surface mixed layer (Kirwan et al., 1978, 1979; Large and Van Loon, 1989; Krauss et al., 1989). Thus, because of the quite large drogue depth of the drifters studied here, we consider the drifter trajectories to be fairly representative, at sufficiently large scales, of the real fluid parcel trajectories.

The trajectories of the three drifters are shown in Fig. 1. The solid line is for drifter NO106, the dashed line for NO307 and the dash-dotted line is

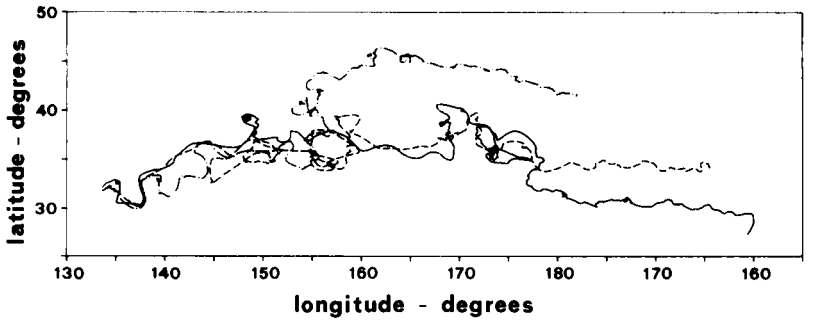


*Fig. 1.* Lagrangian trajectories of the three satellite tracked drifters in the Kuroshio Extension. The solid line is for buoy NO106, dashed line is for NO307 and dash-dotted line is for NO341.

for drifter NO341. Positions of the drifters were determined several times a day by the Nimbus 6 satellite system. The time series were obtained from the raw Nimbus 6 file by interpolation to equally-spaced time intervals of $\Delta t = 12$ h. Additional technical details can be found in Kirwan and Cresswell (1982). The paths begin near latitude 32° North and longitude 133° East near the core of the Kuroshio current. In this region, the Kuroshio is a highly organized flow. During the time of deployment the Kuroshio was evidently in its meander mode as suggested by all 3 drifter paths.

East of the Izu Ridge (approximately 138° East), the Kuroshio flow field is much less organized and highly irregular. Large mesoscale variability in this region is well established; see, e.g., Bernstein and White (1979, 1981), Schmitz (1982) and Schmitz et al. (1982) for analyses based on XBT and current meter data. The intense mesoscale variability of this region is related to several possible effects, including the presence of active mesoscale eddies, turbulent dynamics and Rossby waves. This area is thus appropriate to the study of the properties of fluid parcel trajectories in large-scale flows.

The 3 drifters were deployed within 5 km of each other and within an interval of 2 h; they crossed the Izu Ridge within a 7-day period after following paths that deviated by at most 10 km. However, in the Kuroshio extension region their separations in space and time changed dramatically. In the first few days after crossing the ridge the separation between the drifters grew from approximately 10 to more than 500 km. Thereafter the drifters repeatedly approached and separated in an irregular fashion. It is this extremely irregular and apparently random motion of fluid parcels that is the focus of our study.

## 3. Fractal curves on the plane

In this section we review some of the classical ideas on fractals which are pertinent to this study. The material of this section represents a cursory survey of the techniques which we use in the analysis of the data and is thus limited both in scope and in length. More detailed discussions on fractals and related topics are given in Mandelbrot (1977, 1982). Original developments in the study of the fractal nature of fluid flows may be found for example in Mandelbrot (1972, 1974, 1975), Frisch et al. (1978), Frisch and Morf (1981), and Frisch (1981, 1985) for theoretical aspects and for example in Lovejoy (1982), Lovejoy and Mandelbrot (1985), Sreenivasan and Meneveau (1986), Meneveau and Sreenivasan (1987) and Schertzer and Lovejoy (1987) for experimental results. A recent survey on certain applications of fractals in other fields of physics may be found in Pietronero and Tosatti (1986). For the issues of multifractality, multiple scaling and anisotropy see, e.g., Schertzer and Lovejoy (1983, 1987), Benzi et al. (1984), Frisch and Parisi (1985), Halsey et al. (1986), Lovejoy et al. (1987) and Paladin and Vulpiani (1987).

Heuristically, a fractal is a geometric object whose shape is irregular and/or fragmented at all scales. A technical definition of a fractal is "a set of points whose topological dimension is strictly smaller than its Hausdorff (or fractal) dimen-

sion." The rigorous definition of Hausdorff dimension may be found for example in Mandelbrot (1977, 1982). A striking characteristic of the fractal dimension $D$ is that it can be non-integer. This is in contrast to the topological dimension which is always integer. A fractal curve on a two dimensional surface (for simplicity a plane) has a fractal dimension which lies somewhere between the topological dimension of the curve (which is $D_T = 1$) and the dimension of the space (here 2). A fractal curve is "non-smooth" at every length scale. No matter how small or large a portion of the curve is examined, one always finds finer or larger scale cusps, structures and "wiggles."

The richness of structures in a fractal curve is related to one of the basic properties of fractals, namely their "scaling" behavior. The scaling properties imply that there is a well-defined relationship describing the structure (e.g., the fluctuations) of the curve at different space and time scales. In the present context, we will be concerned with fractal curves whose scaling properties are statistical and in this case the scaling behavior refers to the probability distribution of the random process which generates the curve. If the curve is parameterized by a single scalar (e.g., time) then each component of the curve is a scaling, random scalar function of this parameter.

A more rigorous definition of scaling is now appropriate. This clarification leads to a basic distinction between monofractals (which are also called "simple" fractals) and multifractals. The issues of multiple scaling and of multifractality are relatively recent and may be associated with multiplicative random processes (see, e.g., Schertzer and Lovejoy, 1987 for a discussion of multifractality and for its applications in geophysics), while monofractals are older and simpler mathematical objects associated with additive random processes (e.g., referred to as "scaling of the increments") and have simple scaling rules. In the following we introduce the relevant ideas of fractal mathematics in the context of monofractals. The extension to multifractal behavior is then considered.

In the case of monofractal curves the scaling properties may be related to the self-affine or self-similar character of the curve or of its parametric representations. To properly define self-affinity consider an arbitrary scalar random function of time $X(t)$. If, for an arbitrary interval $\Delta t$,

$$\lambda^{-H}[X(t+\lambda\Delta t) - X(t)] \stackrel{d}{=} [X(t+\Delta t) - X(t)] \quad (3.1)$$

holds independent of time ($\stackrel{d}{=}$ means equality in the sense of distributions), then $X(t)$ is said to be a self-affine simple (or mono) fractal signal with scaling exponent $H$. This exponent must be positive and less than or equal to one. Intuitively a self-affine signal is such that if the time scale is multiplied by a factor $\lambda$ and the signal amplitude by a factor $\lambda^{-H}$ then the transformed time series has the same statistical properties as the original one. It is important to realize here that self-affinity refers to the properties of the differences in the signal amplitudes. Random, self-affine scalar functions with scaling exponent $H$ and gaussian increments are the "fractional Brownian functions" discussed by Mandelbrot (1977, 1982). Ordinary Brownian motion is found when $H = \frac{1}{2}$. Formula (3.1) also indicates that for monofractal curves a single scaling exponent is sufficient to completely define the scaling properties of the system (e.g., the scaling properties of the mean, of the variance, and of higher moments).

Now consider another random process, say $Y(t)$. Being different processes $X(t)$ and $Y(t)$ may have different scaling exponents, say $H_x$ and $H_y$. These two time series can be thought of as the parametric equations of a curve which can be viewed as a self-affine random trajectory on the $X$–$Y$ plane. This is a particular case of anisotropic monofractal curves, and may be found when different physical conditions are acting in different directions. A well-studied, special case of fractal curves are however self-similar (isotropic) fractal curves; this case occurs when $X$ and $Y$ have the same scaling exponent, i.e., $H_x = H_y$. This occurs for example when $X$ and $Y$ are different realizations of the same underlying random process. For self-similar monofractals the fractal dimension of the trajectory is given by

$$D = \min[1/H, 2]. \quad (3.2)$$

Hence for $0 < H < 1$, the trajectory is a simple fractal curve such that $1 < D \leqslant 2$.

The calculation of the scaling exponent just discussed is a common method for determining the scaling properties and for obtaining the fractal dimension of a self-similar monofractal

curve. Another method for obtaining the fractal dimension is based on measuring the length of the curve by varying-length rulers (see Mandelbrot, 1967, 1977, 1982). If the length is approximated by a broken line whose segments have a "yardstick" length $\Delta$ then, in the limit for small $\Delta$, the length goes as

$$L(\Delta) \underset{\Delta \to 0}{\approx} \Delta^{1-D_L}, \tag{3.3}$$

where $D_L$ is the "divider dimension" which approximates the Hausdorff dimension $D$. For an analytic function, $D_L = 1$ and one obtains the ordinary length of a differentiable curve. For fractal curves the length diverges for smaller and smaller yardstick lengths. Computing the power law in (3.3) for the length divergence of a self-similar monofractal curve furnishes its fractal dimension.

A third method for determining the dimension of a fractal curve is based on the computation of the correlation dimension of the curve through a method proposed by Grassberger and Procaccia (1983). To compute the correlation dimension (which is an approximation to the Hausdorff dimension) from a digitized, vector time series $\boldsymbol{x}(t_i)$ one first calculates the Grassberger and Procaccia correlation function

$$C(\varepsilon) = \frac{1}{M^2 - M} \sum_{i \neq j} \Theta(\varepsilon - \|\boldsymbol{x}(ti) - \boldsymbol{x}(tj)\|), \tag{3.4}$$

where $\Theta$ is the Heavyside step function, $M$ is the number of points in the time series and the vertical bars indicate the norm of the vector. In the case of a self-similar fractal curve one has for small $\varepsilon$,

$$C(\varepsilon) \underset{\varepsilon \to 0}{\approx} \varepsilon^{\nu}, \tag{3.5}$$

where $\nu$ is the correlation dimension of the curve. Typically the correlation dimension is computed by calculating the slope of the correlation function (for small $\varepsilon$) in log-log coordinates.

An important observation is that the fractal dimension can be related to concepts from classical time series analysis. Specifically, there is a close relationship between self-affine, monofractal signals $X(t)$ and their power spectra. Self-affinity implies that there is no preferred length scale in the signal. By a straightforward extension of the classic argument which relates the structure function of a signal to its power spectrum (see Panchev, 1971), one finds that a self-affine signal with scaling exponent $H$ has a power law spectrum $P(\omega) \approx \omega^{-\alpha}$ (where $\omega$ is the angular frequency) such that

$$\alpha = 2H + 1, \quad 1 < \alpha \leqslant 3. \tag{3.6}$$

It is possible to extend this result to the case of a curve in an $N$-dimensional space, where one finds that, for self-similar monofractal curves, the spectral slopes of the signal components can be related to the fractal dimension of the curve through (3.2) and (3.6), such that

$$D = \min[2/(\alpha - 1), N]. \tag{3.7}$$

It is important to stress that the relation between the scaling nature of a signal and the power-law dependence of its power spectrum is unidirectional, i.e., the self-affine, fractal character of a signal determines the power law form of the spectrum, and not vice versa. Only in particular cases, in which both the power spectrum and the phase spectrum have particular characteristics, then relation (3.6) is valid in both "directions". An example of this is provided by random systems with power-law spectra and random Fourier phases uniformly distributed on $(0, 2\pi)$ (see, e.g., Osborne and Provenzale, 1989). In this particular case, the slope of the power spectrum and the fact that the phases are random univoquely fixes the self-affine properties of the signal. In general, however, the sole knowledge of power-law dependence in a power spectrum does not infer that the corresponding signal is fractal. In fact (a) perfect power-law spectra are almost never observed in experimental results and one does not know a priori how sensitive the fractal properties are to deviations from power-law behavior, and (b) simple examples exist of signals which have power law spectra but which are *non*-fractal. The common triangular wave has a power law spectrum $P(\omega) \approx \omega^{-2}$ but it is obviously non-fractal. Thus, when an $\omega^{-2}$ spectrum is for example observed, it is not possible to know a priori whether the corresponding signal is self-affine (and fractal) or if it is dominated by few strong "jumps" (and is non-fractal). The fractal nature of a signal must thus be assessed independently from the power-law form of the spectrum. The latter may be taken at most as an indication of the possible presence of fractal behavior.

For simple, self-similar fractal curves the different methods for computing the fractal dimension provide (within the statistical uncertainties associated with the experimental errors and the finite amount of data) the same value for the fractal dimension. This relationship does not hold if the curve under study has a multifractal nature. In this case the parametric representation of the curve does not obey a simple relationship such as eq. (3.1), and the correspondence between the value of the dimension and the logarithmic slope of the power spectra is not necessarily given by eq. (3.7). The different methods for computing the fractal dimension, which rely upon different assumptions and measure different scaling properties of the curve, may thus provide different values for the fractal dimension. This results from the fact that for data with multifractal properties there are infinitely many different fractal dimensions. These are related to the different moments of the probability distributions of the process under study.

Multifractal properties are in fact related to multiplicative random processes and are associated with different scaling properties at different scales. In this case, a single scaling exponent (and a single fractal dimension) are not sufficient to describe the behavior of the statistical moments at different scales (see, e.g., Schertzer and Lovejoy, 1987 and Paladin and Vulpiani, 1987). Thus the extension from the simple scaling properties of monofractals to the more complex situation found for multifractals allows for a wider application of the "fractal approach" and also allows for a closer link to the dynamical processes active in fluid flows.

A simple way to study multifractal behavior is based on the use of a box-counting algorithm. Given a fractal curve on a two dimensional surface (for simplicity a plane) the box-counting procedure is based on filling the plane with a covering of adjacent square boxes of size $\varepsilon$, and on computing the probability $p_i(\varepsilon)$ that the $i$th box contains a piece of the fractal curve. For fractal curves one has that for small $\varepsilon$

$$\sum_i [p_i(\varepsilon)]^q \approx \varepsilon^{(q-1)D_q}, \tag{3.8}$$

where the sum is extended over all non-empty boxes. The quantities $D_q$ are the generalized fractal dimensions; a fundamental difference between monofractals and multifractals is that for monofractal curves one has that $D_q = D_{q'}$ for $q \neq q'$ while for multifractals the different generalized dimensions are not equal. In general in fact $D_q < D_{q'}$ for $q > q'$. The usual correlation dimension is for example recovered for $q = 2$. Thus computing at least some of the generalized dimensions $D_q$ provides a way to test the multifractal nature of a signal.

A word of caution about the application of multifractal methods is perhaps necessary however. The interest herein is focused on the application of these ideas to experimental data. A realistic application of multifractal methods to natural data provides information only on moments of lowest order. It is well-known that the errors of the higher moments may be large because of experimental noise and the finite length of a time series. Another question relates to the origin of (possibly observed) differences among the various generalized dimensions, since it may be unclear whether these deviations are produced by statistical fluctuations or by genuine multifractal behavior. These points will be discussed further below in the analysis of the Kuroshio data.

It is worth stressing that in all physical applications the focus is on "natural" fractals, as opposed to mathematical fractals. The latter "scale" over *all* length scales and their length truly diverges, while the former scale only in a well defined range of scales. For natural fractals small scale processes such as molecular diffusion and experimental noise limit the scaling range for small distances. In fluid dynamics an additional constraint to scaling is provided by the particle paths being solutions to a system of partial differential equations and hence continuously differentiable at very small scales. At large scale constraints such as the finite time of the experimental measurement, or natural boundaries such as the size of the ocean, provide an upper limit to scaling. For natural fractals the various fractal analysis methods therefore provide the value of the fractal dimension and also indicate the scale range over which fractal properties hold. In particular the scaling exponent calculations provide time scale information while the yardstick length and correlation function methods give space scales. Employing the various methods, one can thus gain independent space and time

scale information about the extent of the fractal scaling range. In the authors' opinion the information on the extent of the scaling range is probably almost as important as the discovery of the scaling behavior itself.

## 4. Fractal analysis of the Kuroshio data

In this section, the ideas discussed above are applied to the analysis of the drifter trajectories from the Kuroshio extension. The first test is to compute the scaling exponents $H_x$ and $H_y$ of the longitude ($x$) and latitude ($y$) positions of the drifters. This test is important because it determines whether the signals display (statistical) scaling properties. As discussed above this method also provides time-scale information.

To compute the scaling exponents attention is focused on the average absolute value of displacements in longitude ($\Delta x$) and latitude ($\Delta y$), which for self-affine signals must obey

$$\overline{|x(t+\lambda\Delta t)-x(t)|} = \overline{\Delta x(\lambda\Delta t)} = \lambda^{H_x}\,\overline{\Delta x(\Delta t)} = \lambda^{H_x}\,\overline{|x(t+\Delta t)-x(t)|}, \quad (4.1)$$

$$\overline{|y(t+\lambda\Delta t)-y(t)|} = \overline{\Delta y(\lambda\Delta t)} = \lambda^{H_y}\,\overline{\Delta y(\Delta t)} = \lambda^{H_y}\,\overline{|y(t+\Delta t)-y(t)|}. \quad (4.2)$$

In (4.1) and (4.2), the vertical bars indicate absolute value and the overbar indicates a time average. The delay time $\lambda\Delta t$ is an integer multiple of the sampling time $\Delta t = 12$ hours. If the signals are self-affine then graphs of $\overline{\Delta x(\lambda\Delta t)}$ and $\overline{\Delta y(\lambda\Delta t)}$ versus $\lambda$ must fall on a straight line on a log-log plot, the slope of this line being the value of the scaling exponent.

Figs. 2 and 3 show $\overline{\Delta x(\lambda\Delta t)}$ and $\overline{\Delta y(\lambda\Delta t)}$ versus $\lambda$ in log-log coordinates for each of the drifters. The mean (eastward and northward) drifter velocity has been removed from each time series used here. This step is standard in the study of turbulent flows and in our case it is useful in that it compacts the longitude signals that would otherwise be stretched in the east-west direction by the zonal flow. This implies that we are studying the properties of fluid particle motions around the rectilinear trajectory generated by a constant mean flow. This is also equivalent to a Galilean transformation to a coordinate system moving with the constant mean flow. These aspects are discussed further in Section 5.

From Figs. 2 and 3 scaling is evident both for longitude and latitude for all three drifters. A lower limit to the scaling range is fixed by the deviation of the curve from a straight line to be approximately 1.5 days. An upper limit to scaling is approximately 8 days for longitude and 6.5 days for the latitude time series. Table 1 lists the values of the scaling exponents obtained from a least-square-fit over the scaling range. The indicated uncertainties on the individual values of $H_x$

Table 1. *Values of the scaling exponent and of the fractal dimension obtained by the various methods from the three trajectories*

| Drifter | Component | $H$ | $D = 1/H$ | $D_L$ | $\nu$ |
|---|---|---|---|---|---|
| NO106 | longitude | $0.85 \pm 0.02$ | | | |
| | latitude | $0.73 \pm 0.02$ | | | |
| | average | $0.79 \pm 0.06$ | $1.27 \pm 0.09$ | $1.20 \pm 0.03$ | $1.35 \pm 0.05$ |
| NO307 | longitude | $0.85 \pm 0.02$ | | | |
| | latitude | $0.84 \pm 0.02$ | | | |
| | average | $0.84 \pm 0.02$ | $1.19 \pm 0.02$ | $1.14 \pm 0.02$ | $1.28 \pm 0.08$ |
| NO341 | longitude | $0.75 \pm 0.02$ | | | |
| | latitude | $0.75 \pm 0.02$ | | | |
| | average | $0.75 \pm 0.02$ | $1.34 \pm 0.04$ | $1.35 \pm 0.05$ | $1.33 \pm 0.04$ |
| ensemble average | longitude | $0.81 \pm 0.03$ | | | |
| | latitude | $0.77 \pm 0.03$ | | | |
| | average | $0.79 \pm 0.03$ | $1.26 \pm 0.05$ | $1.23 \pm 0.06$ | $1.32 \pm 0.06$ |

The uncertainties on the individual values are the least-square-fit statistical bounds, while the uncertainties on the average values are the maximum between the error due to propagation of individual errors and the standard deviation of the average.

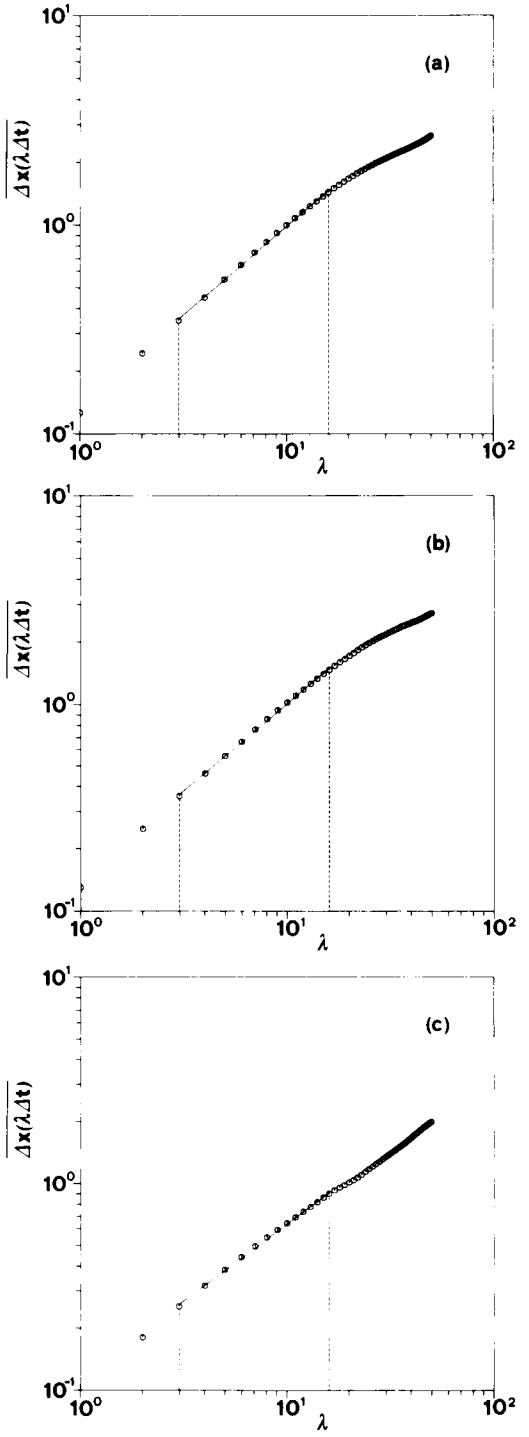


*Fig. 2.* Plot of $\overline{\Delta x(\lambda\Delta t)}$ versus $\lambda$ in log-log coordinates for the three drifter trajectories. Panel (a) is relative to drifter NO106, panel (b) refers to drifter NO307 and panel (c) to drifter NO341. The two vertical dashed lines indicate the limits of the scaling range. The solid line in each panel is the least-square fit to the data. The slope of this line gives the scaling exponent.

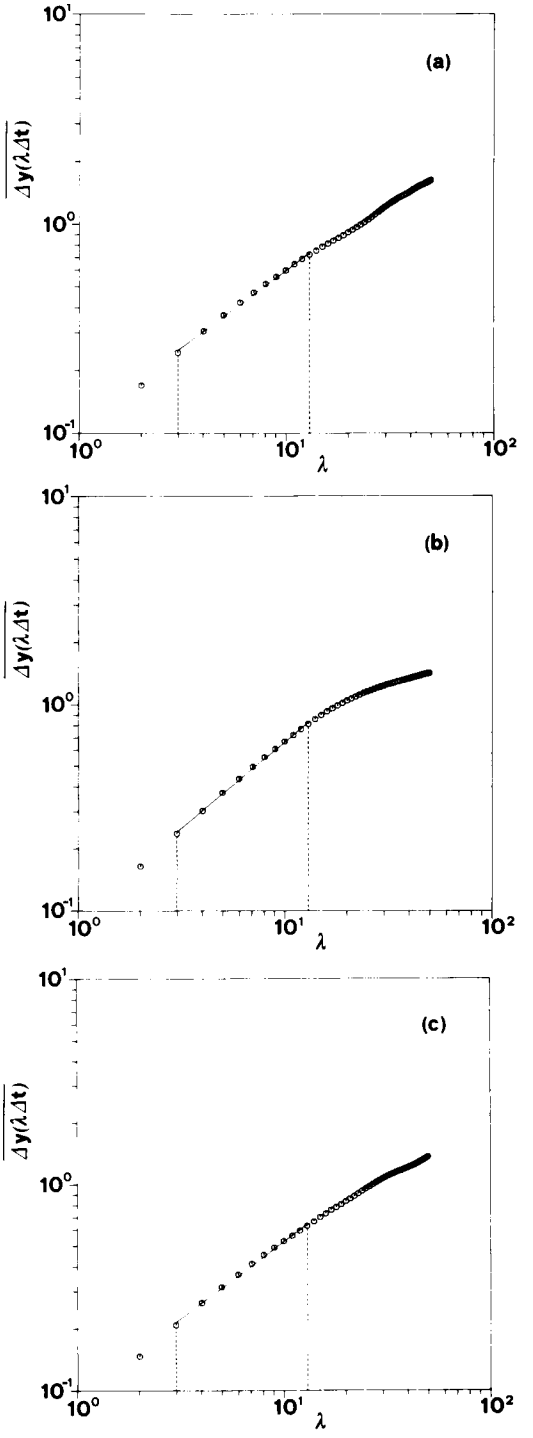


*Fig. 3.* Plot of $\overline{\Delta y(\lambda\Delta t)}$ versus $\lambda$ in log-log coordinates for the three drifter trajectories. Same details as in Fig. 2.

and $H_y$ are the statistical errors of the least square fits to the slopes of $\overline{\Delta x(\lambda \Delta t)}$ and $\overline{\Delta y(\lambda \Delta t)}$. These have been obtained as the least-squares 95% confidence limits on the individual values of the slope. It should be recognized that these are just the statistical uncertainties on the power law dependence of $\overline{\Delta x(\lambda \Delta t)}$ and $\overline{\Delta y(\lambda \Delta t)}$, they do not account for bias in the calculations arising from the fact that the time series have finite length, for propagation of experimental errors or, even more importantly, for the statistical fluctuations inherent in the value of the scaling exponent from one signal (and hence one realization) to another. This latter point is discussed further in Section 5. We remark here that when an average over several individual values of the scaling exponent (or of the dimension) is taken, the indicated uncertainty is the maximum between the standard deviation of the average and the uncertainty due to propagation of individual least-square errors. The latter is in general observed to be much smaller than the former.

Averaging the longitude and latitude scaling exponents for each drifter and using eq. (3.2) gives estimates of the fractal dimension of each of the three trajectories. These are also reported in Table 1. The average over all drifters then furnishes a value $D = 1.26 \pm 0.05$ for the average fractal dimension. This result is evidently the first indication that fluid parcel trajectories in a large scale ocean flow may exhibit fractal and scaling behavior.

The average over $H_x$ and $H_y$ for each trajectory and the use of eq. (3.2) implies an isotropic character for the buoy trajectories. This seems justified since the difference between the average longitudinal and latitudinal values of the scaling exponent is quite small, indicating that any deviations from isotropic behavior are probably very mild. We thus consider the drifter trajectories, at least in a first approximation, to be isotropic fractal curves. We note however that the effects of rotation induce well-known differences between the meridional and the zonal directions, which could in turn induce different scaling properties in the two directions and consequently result in anisotropic behavior (which could for example be studied by methods such as "functional box counting", see, e.g., Lovejoy et al. (1987), and Schertzer and Lovejoy (1987)). A deeper understanding of the isotropic or anisotropic nature of drifter trajectories in large scale flows is thus an important issue, but definite conclusions must be deferred to future studies with larger data bases than those considered here.

As a second step in the study of the fractal properties of these data we now compute the lengths of the three drifter trajectories in the $x$-$y$ plane by a variation of the yardstick method discussed earlier in Section 3. The strict version of this method cannot be applied here since the data are equally spaced in time but not in space. This means that one cannot choose a fixed yardstick length. The simplest solution to this problem is to compute the trajectory length $L(\Delta_{av})$ versus the average length $\Delta_{av}$ of the yardstick. A separate analysis shows that the errors introduced by a non-constant yardstick length are, in the present case, on the order of the statistical uncertainties of the least-square fit to the slope in the scaling region. Thus the slope of $L(\Delta_{av})$, for small $\Delta_{av}$, gives the fractal dimension of the curve with inconsequential error.

Fig. 4 shows the results for the three drifter trajectories. The path lengths clearly diverge for small $\Delta_{av}$. In this region all curves exhibit power-law behavior with $L(\Delta_{av}) \sim \Delta_{av}^{1-D_L}$. The values of $D_L$ are listed in Table 1. These results give as an average fractal dimension $D_L = 1.23 \pm 0.06$ for the three trajectories. Of course with these data (as with all experimental time series) the length divergence does not continue up to infinitesimal yardstick lengths. The length divergence follows a well-defined power law down to scales of roughly 20 km, indicating fractal and scaling behavior down to these spatial scales. An upper limit to scaling may in turn be fixed at approximately 100 km.

The last test which we use for determining the value of the fractal dimension (and for estimating the extent of the scaling range) is obtained from the Grassberger and Procaccia correlation function. Fig. 5 shows the 3 correlation functions for the drifter paths. The mean drifter velocity was removed from the data before calculation of the correlation function. Scaling is evident from spatial scales of approximately 20 km up to scales of roughly 150 km. The slopes of the three correlation curves (in log-log coordinates) in the scaling range and the individual least-square-fit errors are given in Table 1. From these values the average correlation dimension of the three drifter trajectories is calculated to be $\nu = 1.32 \pm 0.06$.

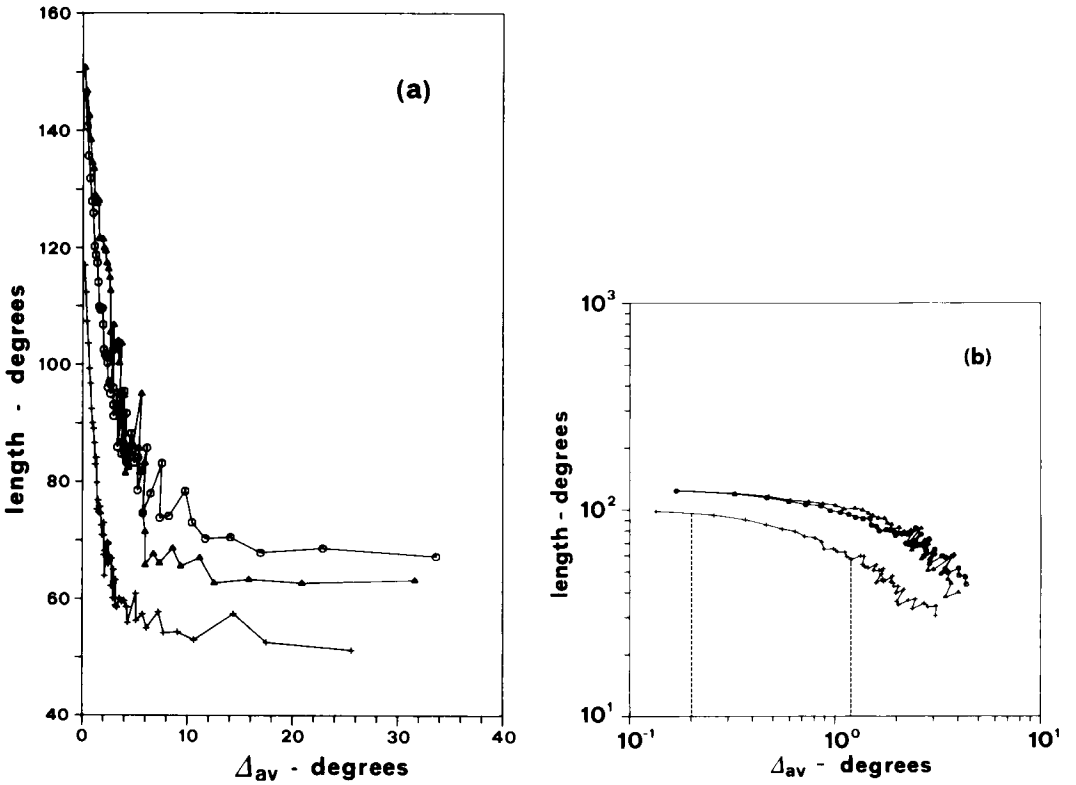


*Fig. 4.* Length $L(\Lambda_{av})$ of the three trajectories versus the average yardstick length in linear coordiantes (panel (a)) and log-log coordinates (panel (b)). Circles are for buoy NO106, triangles for NO307 and crosses for NO341. Note the divergence of the lengths for small $\Lambda_{av}$.

We have therefore used three independent methods for finding the value of the fractal dimension and the extent of the scaling range. Since the 3 methods rely upon different assumptions, and because they measure different properties of the trajectories, the likelihood is lessened that systematic factors associated with a particular technique have affected the results of the analysis. All 3 methods show that the drifter trajectories display fractal properties and scaling in a well-defined range of scales. Estimates of the average fractal dimension are between 1.23 and 1.32. The differences among the results of the various methods, as well as the differences among the estimates obtained from different drifter trajectories, are discussed in Section 5.

Previously it was noted that the fractal dimension of a self-affine monofractal signal is related to the logarithmic slope of its power-law spectrum. This is due to the fact that the scaling nature of a signal originates a power spectrum with power-law behavior. Power spectral analysis of the drifter positions is shown in Fig. 6 for the longitude and in Fig. 7 for the latitude time series. Even if not perfectly power-law as would be found for "mathematical" fractals, the spectra of the drifter positions clearly display an overall power-law dependence. The spectra displayed here have been passed through a Hanning filter. The spectra have been fitted to power laws by the least-squares method over the range 0.04–1.0 rad/day. We note that in analyses like those considered here, considerable care must be exercised in computing the slopes of the power spectra. Procedures such as the Hanning filter may in fact lead to biased estimates of the spectral slope. For this reason the slope estimates reported here were obtained from the unfiltered

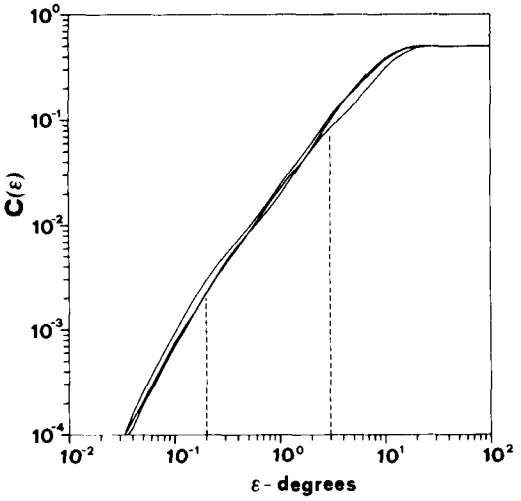


*Fig. 5.* Correlation functions for the three drifter trajectories. The slope of the correlation function in log-log coordinates is a measure of the correlation dimension of the signal. The two vertical dashed lines indicate the approximate limits of the scaling range.

spectra. The resultant slopes are given in Table 2 where the uncertainties are the 95% confidence limits of the least-square slope estimates. We also provide estimates of spectral slopes derived from the values of the scaling exponents and the fractal dimension (through eqs. (3.6) and (3.7)); these are also given in Table 2. Note that these latter are all within the 95% confidence limits of the observed slopes. This relation between the self-affine character of the signals and the power-law dependence of their spectra was in fact expected on the basis of the discussion given in Section 3, and may be considered as a further confirmation of the scaling nature of these data.

Given that the scaling and fractal nature of drifter trajectories in large-scale ocean flows has been determined, an interesting question is now whether they also display a monofractal or a multifractal behavior. To this end we have applied a box-counting algorithm to the detrended drifter data in order to determine the generalized dimensions $D_q$ for several values of $q$. From an experimental point of view, the probability $p_i(\varepsilon)$ that the $i$th box with size $\varepsilon$ be occupied is now empirically computed from a measured series of points by

$$p_i(\varepsilon) = n_i(\varepsilon)/N, \tag{4.3}$$

where $n_i(\varepsilon)$ is the number of data points falling in the $i$th box and $N$ is the total number of points in the time series.

For determining the possible multifractal behavior of the drifter data, we have computed the function $\sum_i [p_i(\varepsilon)]^q$ for several values of $q$ between 1.5 and 6.5 for each of the trajectories. Power-law behavior for all three trajectories and for all the selected values of $q$ is evident in the functions

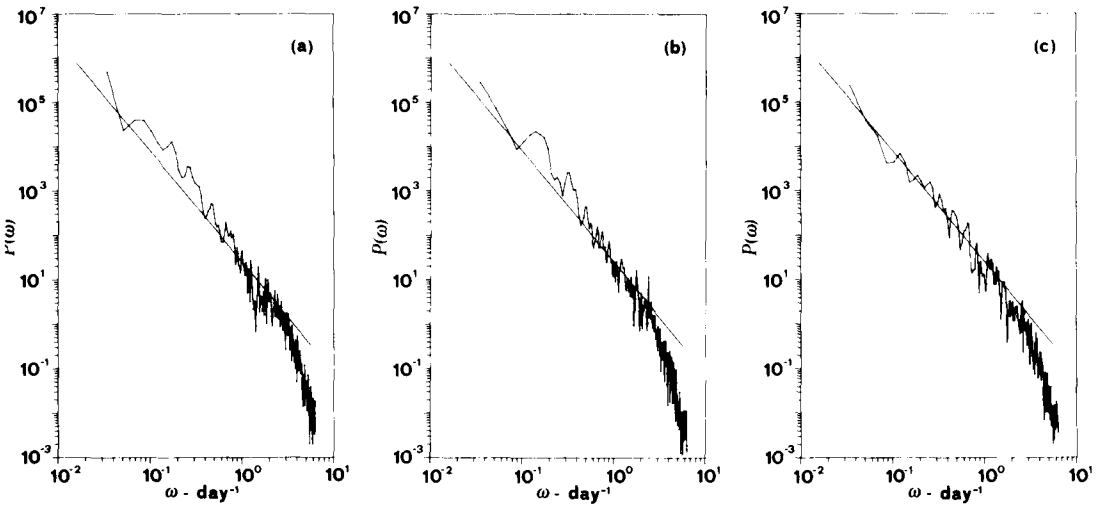


*Fig. 6.* Power spectra of longitude signals for the three drifter trajectories. Panel (a) refers to drifter NO106, panel (b) to drifter NO307 and panel (c) to drifter NO341. The solid line represents an $\omega^{-2.5}$ power spectrum.

Table 2. *Values of the spectral slopes measured from the drifter spectra through least-square fits and of the spectral slopes derived from the self-affine character of the signal*

| Drifter | Component | $\alpha$ | From $H$ | From $D_L$ | From $\nu$ |
|---|---|---|---|---|---|
| NO106 | longitude | $2.75 \pm 0.37$ | $2.69 \pm 0.03$ | | |
| | latitude | $2.11 \pm 0.42$ | $2.46 \pm 0.05$ | | |
| | average | $2.43 \pm 0.40$ | $2.58 \pm 0.12$ | $2.67 \pm 0.04$ | $2.48 \pm 0.06$ |
| NO307 | longitude | $2.78 \pm 0.37$ | $2.69 \pm 0.03$ | | |
| | latitude | $2.49 \pm 0.37$ | $2.68 \pm 0.04$ | | |
| | average | $2.64 \pm 0.37$ | $2.69 \pm 0.04$ | $2.75 \pm 0.04$ | $2.56 \pm 0.10$ |
| NO341 | longitude | $2.56 \pm 0.34$ | $2.49 \pm 0.03$ | | |
| | latitude | $2.23 \pm 0.39$ | $2.49 \pm 0.05$ | | |
| | average | $2.40 \pm 0.37$ | $2.49 \pm 0.04$ | $2.48 \pm 0.05$ | $2.51 \pm 0.05$ |
| ensemble average | longitude | $2.70 \pm 0.36$ | $2.63 \pm 0.07$ | | |
| | latitude | $2.28 \pm 0.39$ | $2.54 \pm 0.07$ | | |
| | average | $2.49 \pm 0.38$ | $2.59 \pm 0.07$ | $2.63 \pm 0.07$ | $2.51 \pm 0.07$ |

The indicated uncertainties on the observed spectra are the least-square-fit statistical bounds while those on the computed slopes are due to propagation of the errors of the scaling exponent and of the fractal dimension.

$\sum_i [p_i(\varepsilon)]^q$ at least for $\varepsilon$ in the interval from approximately 20 to more than 100 km (in agreement with the results of the methods discussed above) and the generalized dimensions are reported in Table 3. Fig. 8 reports the generalized dimension $D_q$ versus $q-1$ for the drifter NO106 (panel a), for NO307 (panel b) and for NO341 (panel c).

We recall that for monofractals, the generalized dimensions $D_q$ are all equal. From Fig. 8 we see however that there is a well-defined decrease of the $D_q$ for increasing $q$, a common result in the case of multifractal curves. Note that the three different trajectories provide quite consistent estimates of the generalized dimensions. Note also however that the average $D_q$ varies only from $D_{1.5} \approx 1.4$ to $D_{6.5} \approx 1.2$, i.e., less than 20%. While obviously constrained to lie in the range $1 \leqslant D_q \leqslant 2$, one would have expected a larger variation for "strong" multifractal behavior. We thus conclude that the drifter trajectories probably possess a genuine multifractal

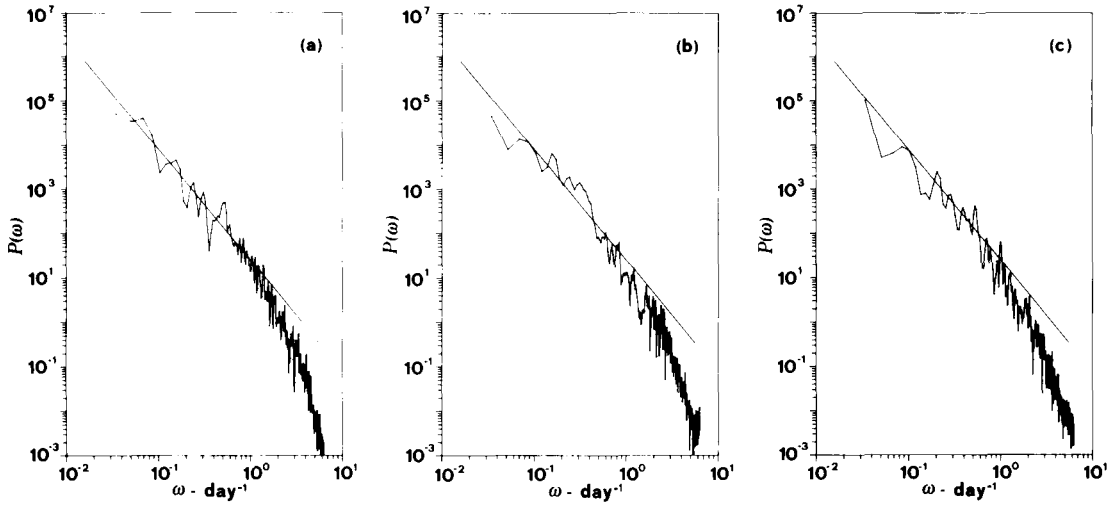


*Fig. 7.* Power spectra of latitude signals for the three drifter trajectories. Same details as Fig. 6.

Table 3. *Values of the generalized fractal dimensions obtained by a box counting method from the three trajectories*

| | Generalized dimension $D_q$ | | |
|---|---|---|---|
| $q-1$ | NO106 | NO307 | NO341 |
| 0.50 | 1.38 ± 0.02 | 1.44 ± 0.03 | 1.37 ± 0.03 |
| 0.75 | 1.36 ± 0.02 | 1.42 ± 0.03 | 1.35 ± 0.03 |
| 1.00 | 1.34 ± 0.02 | 1.40 ± 0.03 | 1.33 ± 0.03 |
| 1.25 | 1.32 ± 0.02 | 1.38 ± 0.04 | 1.32 ± 0.03 |
| 1.50 | 1.30 ± 0.02 | 1.36 ± 0.04 | 1.30 ± 0.03 |
| 1.75 | 1.28 ± 0.02 | 1.34 ± 0.04 | 1.28 ± 0.03 |
| 2.00 | 1.27 ± 0.02 | 1.32 ± 0.05 | 1.27 ± 0.03 |
| 2.25 | 1.26 ± 0.02 | 1.31 ± 0.05 | 1.26 ± 0.03 |
| 2.50 | 1.24 ± 0.02 | 1.29 ± 0.05 | 1.25 ± 0.04 |
| 2.75 | 1.23 ± 0.02 | 1.28 ± 0.06 | 1.23 ± 0.04 |
| 3.00 | 1.22 ± 0.02 | 1.26 ± 0.06 | 1.22 ± 0.04 |
| 3.25 | 1.21 ± 0.02 | 1.25 ± 0.06 | 1.21 ± 0.04 |
| 3.50 | 1.20 ± 0.03 | 1.24 ± 0.06 | 1.20 ± 0.04 |
| 3.75 | 1.20 ± 0.03 | 1.23 ± 0.07 | 1.20 ± 0.04 |
| 4.00 | 1.19 ± 0.03 | 1.22 ± 0.07 | 1.19 ± 0.04 |
| 4.25 | 1.18 ± 0.03 | 1.21 ± 0.07 | 1.18 ± 0.04 |
| 4.50 | 1.18 ± 0.03 | 1.20 ± 0.07 | 1.18 ± 0.05 |
| 4.75 | 1.17 ± 0.03 | 1.19 ± 0.07 | 1.17 ± 0.05 |
| 5.00 | 1.16 ± 0.03 | 1.19 ± 0.07 | 1.16 ± 0.05 |
| 5.25 | 1.16 ± 0.03 | 1.18 ± 0.08 | 1.16 ± 0.05 |
| 5.50 | 1.15 ± 0.03 | 1.17 ± 0.08 | 1.15 ± 0.05 |

The uncertainties on the individual values are the least-square-fit statistical bounds.

behavior, which is however quite "mild". This also implies that, while multiplicative random processes are probably required for a deeper understanding of the dynamics, a simple first-order model based on additive processes (e.g., fractional Brownian motion) probably describes some of the principal features of the drifter motions.

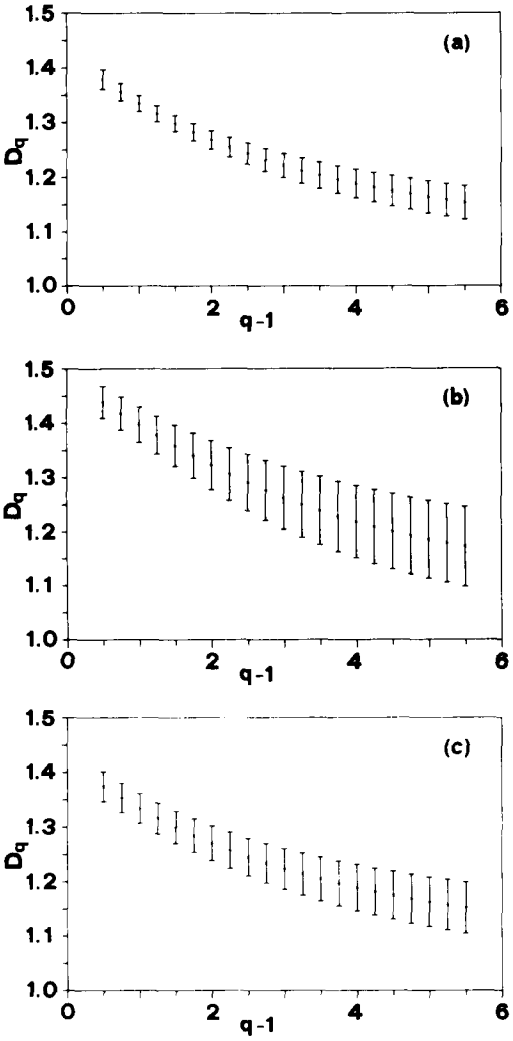


*Fig. 8.* Generalized dimensions $D_q$ versus $q-1$. Panel (a) refers to drifter NO106, panel (b) to drifter NO307 and panel (c) to drifter NO341.

## 5. Discussion of uncertainties in the analysis of the data

Table 1 summarizes our analysis on the monofractal properties of the three drifter trajectories. These results indicate that near-surface fluid particle paths from the Kuroshio extension region exhibit fractal behavior with an average fractal dimension of 1.27 ± 0.06 for spatial scales from approximately 20 to 150 km and time scales from approximately 1.5 days to 1 week. This value of the fractal dimension has been obtained by averaging the dimension estimates from three independent methods and the indicated uncertainty is the standard deviation of the average. Statistical bounds on the value of the average fractal dimension of the drifter paths may be fixed by the use of a standard two-tailed student-$t$ distribution. Averaging the dimension estimates from the three different methods and the three trajectories one obtains $D = 1.27 \pm 0.11$ with a 95% confidence limit. It is important to stress

that the 95% confidence limits outlined above indicate that the average fractal dimension is significantly larger than one. This is important since it provides strong evidence for the fractal character of the drifter trajectories.

The individual values of the fractal dimension and of the scaling exponent have been determined by fixing a scale range over which an appropriate quantity ($\overline{\Delta x(\lambda \Delta t)}$, $\overline{\Delta y(\lambda \Delta t)}$, $L(\Delta_{av})$, $C(\varepsilon)$) shows a power-law dependence on its argument. The choice of the scaling range is, of course, somewhat subjective. We observe however that if we decrease the range of scales over which the least-square fit to the data has been obtained, no significant changes in the values of the scaling exponent are observed. If, on the contrary, we perform a least-square fit in a range larger than that selected in the analysis, then significant changes in the values of the scaling exponent and much larger errors on the least-square fits are soon observed. Thus in general the idea that guides the search for the extension of the scaling range is to define the maximum range inside which no significant deviations from power law dependence are detected. The smallness of the statistical errors on the least-square fits to the slopes (which in the present case never exceeds 4% of the value of the scaling exponent) in particular provides a strong indication that $\overline{\Delta x(\lambda \Delta t)}$ and $\overline{\Delta y(\lambda \Delta t)}$ obey a power law and thus that the scaling nature of these signals is well defined.

Another important issue in the analysis is whether the differences among the fractal dimension estimates provided by the various methods and by the different trajectories are significant. From Table 1, it is seen that of the three methods used to compute the fractal dimension, the "yardstick length" ($D_L$) method gives results with the largest scatter. The most internally consistent technique for obtaining the fractal dimension for this data set has been found to be the correlation dimension ($\nu$) method. The use of individual least-square errors is however inappropriate to decide whether the deviations among the various measured values of the fractal dimension may have some significance, as these errors only indicate the correctness of a power-law fit to each individual signal and do not take into account experimental errors, biases arising from the relatively limited number of data points and

Table 4. *Values of the scaling exponent obtained from fifteen different realizations of a self-affine random signal with 733 points*

| Realization number | Scaling exponent |
|---|---|
| 1 | $0.777 \pm 0.005$ |
| 2 | $0.816 \pm 0.003$ |
| 3 | $0.682 \pm 0.010$ |
| 4 | $0.779 \pm 0.002$ |
| 5 | $0.851 \pm 0.004$ |
| 6 | $0.797 \pm 0.005$ |
| 7 | $0.756 \pm 0.003$ |
| 8 | $0.704 \pm 0.006$ |
| 9 | $0.764 \pm 0.004$ |
| 10 | $0.796 \pm 0.003$ |
| 11 | $0.787 \pm 0.006$ |
| 12 | $0.789 \pm 0.004$ |
| 13 | $0.787 \pm 0.002$ |
| 14 | $0.772 \pm 0.008$ |
| 15 | $0.659 \pm 0.016$ |

The uncertainties on each value of $H$ are the least-square fit statistical bounds. It is clear how the value of $H$ displays statistical fluctuations from one realization to another which are not accounted for by the least-square fit statistical bounds.

statistical fluctuations of the measured dimension from one signal to another. Hence the errors of the least-square fits to the slopes, while being important indicators of the well-defined scaling properties of the signals, are too small to be considered as representative of the real statistical fluctuations in the value of the scaling exponent from one signal (i.e., one statistical realization) to another. To emphasize this observation, we report in Table 4 the values of the scaling exponent computed from fifteen realizations of a synthetic, self-affine random process (with 733 data points) obtained by inverting a power-law power spectrum $P(\omega) \approx \omega^{-2.7}$ with random Fourier phases uniformly distributed on $(0, 2\pi)$. As discussed above, for this particular class of random processes there is a one-to-one correspondence between the slope of the power spectrum and the value of the scaling exponent. Each realization of this process corresponds to the same power spectrum but to a different set of random phases. From Table 4, one sees that the values of the scaling exponent obtained from the various realizations are well outside the respective least-square confidence limits, thus indicating

that these must be considered at most as lower limits to the real statistical fluctuations of the system. A similar behavior is therefore to be expected in general when the scaling exponent (or the fractal dimension) is measured from experimental data, even if arising from a strict deterministic origin, as the measurement process itself would generate fluctuations in the values of these quantities.

To study the significance of the deviations observed among the various measured values of the fractal dimension one may thus more appropriately use a standard two-tailed, student-$t$ distribution for determining the confidence limits of each group of measurements and for testing their consistency. Averaging the dimension estimates obtained by the three different methods for each of the trajectories, or alternatively averaging over the trajectories to keep distinct the outputs of the various methods, we find that the various estimates for the fractal dimension are inside the respective 95% confidence limits and differ from each other by at most 10%. It is thus encouraging that for these data from a natural, uncontrolled system the deviations among the fractal dimensions provided by different approaches and by different trajectories are quite small. This suggests that the value of the fractal dimension determined here may be a fundamental property of the flow investigated.

The fact that the dimension estimates provided by the different methods are statistically equivalent is in agreement with the "mild" multifractal behavior determined through a box-counting method, the results of which are reported in Table 3. Computing the generalized dimension $D_q$ we have found that they differ from each other by at most 20% in the range $1.5 \leqslant q \leqslant 6.5$. It cannot be excluded however that the differences among the various $D_q$s could be explained by statistical fluctuations introduced by the finite length of the time series. However the fact that there is a well-defined trend in the dependence of the $D_q$s from $q$, seems to indicate a genuine, even if slight, multifractal nature for the drifter data.

Important technical questions concern the independence of the results of this analysis from both (a) the number of points in the time series and (b) the procedure of mean drift removal. If the drifter trajectories are cut into two or three parts and the various fractal analysis methods are applied to each part, then the dimension estimates obtained in this way randomly differ by at most 15% from the original values. These fluctuations are consistent with the statistical uncertainties observed in our analysis, and are thus neglected in a first approximation. The smallness of the fluctuations in the value of the fractal dimension is important because it indicates that the fractal and scaling properties are nearly uniform over the entire trajectories. Another interesting question relates to whether one may be able to detect small but significant fluctuations of the fractal dimension in different oceanic regions. Although challenging, the answer to this question cannot come from the present analysis as it requires a much larger data base than available here.

Another important point concerns the removal of the mean drift current. Since we are primarily interested in scales between approximately 20 and 200 km, it seems natural to limit the effects of large scale advection, and consequently to consider some form of mean drift removal, especially for the longitude signals. In a first approximation these signals may be represented as a fluctuating part (which is the one of interest here) superimposed onto a monotonically increasing part which mimics the average advective effect of the mean flow. Removal of the mean flow is standard in the study of turbulence. We used several procedues for mean drift removal in our analysis (e.g., removing the mean velocity from the signals, or removing the linear least-square-fit trend, etc.) and in all cases we have found consistent results for the fractal dimension and the scaling exponents. The analysis of the raw data by contrast (i.e., with no mean drift removal) systematically furnished slightly lower values for the fractal dimension, a fact which is related to the systematically larger (of the order of 10%) value of the longitudinal scaling exponent $H_x$.

This behavior is entirely understood as spuriously generated by the "stretching" of the signal due to the mean drift and is observed in general when a fractal curve is subjected to some form of stretching along one of the dimensions. We have investigated this effect by generating a two dimensional self-similar fractal curve with a given and known dimension and then adding a linearly increasing function of time to one of its

components. This resulted in a (spurious) increase of the associated scaling exponent similar to that found in our data analysis. Thus a procedure of mean drift removal seems appropriate in our case. We notice also that the stretching of the trajectories in the mean flow is not directly related to the effects of rotation and to a possible anisotropic nature of fluid particle paths in mesoscale flows. The longitudinal elongation of the trajectories is in fact entirely produced by the advection due to the mean current. For drifter trajectories obtained in currents with a north–south orientation for example the stretching is in the latitudinal direction, with no relationship associated with the effects of rotation. It is conceivable however that an anisotropy might exist in the detrended data, since in general the variance in the east–west direction is larger (by a factor of two or three) than the variance in the meridional direction. Since however an anisotropy in the scaling behavior of the drifter data herein considered is indicated by only one of the three trajectories (NO106), we defer the important study of anisotropic scaling behavior to future analyses with larger amounts of data.

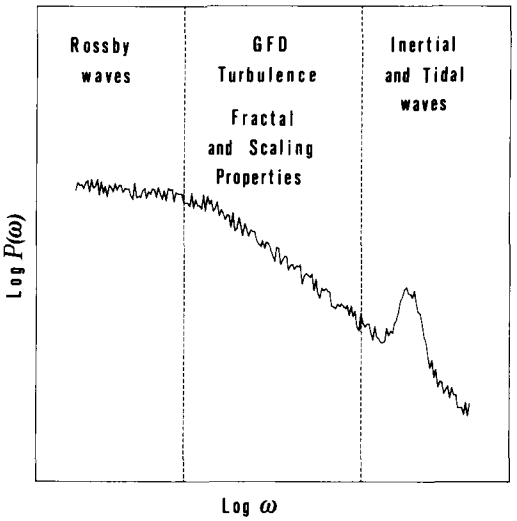


*Fig. 9.* Schematic power spectrum representing the different dynamical domains present in the time scales tested by the drifter trajectories.

## 6. Discussion of physical implications

The fractals encountered in this study are natural fractals, as the scaling properties have been detected only in a limited (but well-defined) range of scales. An important point is now whether the limits to the scaling range are generated by statistical fluctuations and/or experimental considerations or if they reflect some fundamental dynamical limit. Basic dynamical processes active in the flow may in fact be responsible for a finite scaling range. A particular dynamical regime (active on a certain range of scales) may generate fractal behavior in its domain of validity, while other regimes (active at different scales) may be non fractal. In this case the fractal and scaling properties would be dynamically confined to a finite range of scales. The fact that certain experimental data have fractal and scaling properties over a finite range of scales may thus be an important dynamical result. Quantitatively relating the fractal properties to the actual dynamical processes active in a particular flow and carefully exploring the origin of the finiteness of the scaling range are thus major challenges for future theoretical and experimental studies.

In the case of the data analyzed here the scale estimates determined above give a "turbulent intensity" of 15 to 20 cm/s and are in general consistent with usually accepted bounds on geostrophic or quasigeostrophic turbulence. Thus a plausible inference is that the near-surface mesoscale motions in the Kuroshio Extension exhibit fractal behavior in a range of scales usually attributed to geostrophic turbulence. Fig. 9 schematically shows a power spectrum typical of large-scale flows. For scales larger than 10 days and 100 to 200 km, the dynamics are essentially governed by Rossby waves and zonal flows. Our analysis gives no evidence of fractal and scaling properties in this regime. At the opposite side of the spectrum, i.e., for scales shorter than 2 days and 20 km, where inertial and/or tidal-wave dynamics dominate, a lack of fractal and scaling properties is observed. Between these two extreme wave regimes, the dynamics is governed by GFD turbulence and the power spectrum is thought to have a power law dependence (see, e.g., Rhines (1979) and Salmon (1982)). It is in this intermediate range of scales that we find evidence of fractality and scaling. Outside the

GFD turbulence scale range, i.e., in the Rossby or inertial/tidal wave regimes, wave dynamical processes may act to inhibit fractal behavior. In this regard it is interesting to recall a suggestion by Mandelbrot (1977, 1982) that in a Lagrangian framework one difference between laminar and turbulent flows may be in the contrast between the regular and fractal aspects of fluid parcel trajectories. Our findings apparently point in this direction also. We caution however that the limits to the scaling range determined here are essentially indicative; the drifter data are not inconsistent with the existence of a much larger scaling region. In this case, the limits of the scaling range would be of instrumental or statistical origin. In particular the lower limit to scaling could have been artificially generated by, e.g., the finite sampling time or by the positioning errors of the drifter-satellite system. Further work with other data sets is required to clarify this important issue.

A further interesting observation is that the fractal dimension of the trajectories is less than two. This implies that the drifter motions are definitely different from ordinary Brownian motion (for which $D = 2$) and that, if a stochastic model is used to describe the drifter paths, it must possess some form of persistency or "memory" which is not found in Brownian random walks. The fact that $D < 2$ also implies that the drifter motions do not explore and fill the entire plane of the ocean surface, as would be done by Brownian motion.

The principal results obtained here are summarized as follows. Each of the 6 signals has been analyzed by four different methods to determine fractal behavior. Remarkable consistency has been found in the results, which indicate a fractal nature for the drifter trajectories in the range of scales typical of GFD turbulence. It is encouraging that data from a large-scale natural flow, analyzed with four independent techniques, give the same fractal properties. Because these observations come from an uncontrolled experiment in a natural environment, this consistency could not be assumed a priori. We also note that this is evidently the first experimental indication that fluid parcel trajectories in large-scale flows can exhibit fractal behavior. The drifter trajectories have also been shown to possess a "mild" multifractal character. While in general the introduction of multifractility (associated with multiplicative random processes) is an important step toward the understanding of the links between fractal behavior and dynamical processes, for the particular data set studied here, we observe that a satisfactory first-order approximation is probably represented by simple additive processes such as fractional Brownian motions.

We hope that the results discussed here will provide a stimulus to search for fundamental reasons why fractal behavior might occur in flows of this type. A number of important questions are still to be answered. How fundamental dynamical motions generate fractal behavior remains in fact an open crucial question. The implications from a growing body of literature (see, e.g., Mandelbrot, 1974, 1975, 1977, 1982; Frisch et al., 1978; Frisch, 1985; Frisch and Parisi, 1985; Lovejoy and Mandelbrot, 1985; Sreenivasan and Meneveau, 1986; Meneveau and Sreenivasan, 1987; Schertzer and Lovejoy, 1987; Paladin and Vulpiani, 1987) are that there are several deep connections between the nonlinear dynamics generated by the partial differential equations of motion and fractal properties. While these connections are still to be understood it is to be expected that further theoretical clarification is forthcoming. For these reasons, it is important, in our opinion, to continue and to expand on experimental studies which can help shed light on the various aspects of fractal properties and to perhaps provide some insight about possible directions in which theoretical investigations might most fruitfully go. Several important physical questions are open in this context, such as for example: (1) Is the observed value of the fractal dimension common to all fluid parcel trajectories in GFD turbulent flows? How much different is the case of three dimensional turbulence? (2) Are the power spectra obtained for these data typical of Lagrangian GFD turbulence and may they be directly derived through some cascading argument? (3) Are the multifractal properties important and can they be stronger than those determined here? (4) Are the drifter motions (around the mean flow) isotropic or anisotropic? (5) Can one identify the scaling properties of the underlying (Lagrangian) equations of motion? Is it possible to derive the value of the fractal dimension from the equations of motion? (6) Can the drifter trajectories be modeled by (non-

gaussian) stochastic approaches or is there the need for a truly nonlinear deterministic model? (7) What is the relationship between the fractal behavior and the statistical properties of the system? Although these, and many other, fundamental issues are still to be addressed, we believe that the study of the fractal and scaling behavior of large-scale flows in a Lagrangian framework may provide added insight into the fundamental properties of large-scale motions.

## 7. Acknowledgements

We acknowledge Professor C. Castagnoli, Director of the Istituto di Cosmo geofisica del Consiglio Nazionale delle Ricerche, for continuing support and valuable encouragement. This research has received funding from the Consiglio Nazionale delle Ricerche and from the Ministero della Pubblica Istruzione. A. D. Kirwan gratefully acknowledges the support of the Office of Naval Research (Contract N00014-89-J-1595) and of the National Science Foundation (Grant OCE8811453) and the Samuel L. and Fay M. Slover endowment to Old Dominion University. During part of this research A. Provenzale was supported by a fellowship from the "Dottorato di Ricerca in Fisica" at the University of Torino, Italy.

## REFERENCES

Benzi, R., Paladin, G., Parisi, G. and Vulpiani, A. 1984. On the multifractal nature of fully developed turbulence and chaotic systems. *J. Physics A17*, 3521–3531.

Bernstein, R. L. and White, W. B. 1979. Zonal variability in the distribution of eddy energy in the mid-latitude North Pacific Ocean. *J. Phys. Oceanogr. 7*, 123–126.

Bernstein, R. L. and White, W. B. 1981. Stationarity and traveling mesoscale perturbations in the Kuroshio extension current. *J. Phys. Oceanogr. 11*, 692–704.

Davis, R. E. 1982. On relating Eulerian and Lagrangian velocity statistics: single particles in homogeneous flows. *J. Fluid Mech. 114*, 1–26.

Davis, R. E. 1983. Oceanic property transport, Lagrangian particle statistics, and their prediction. *J. Mar. Res. 41*, 163–194.

Davis, R. E. 1985. Drifter observations of coastal surface currents during CODE: The statistical and dynamical views. *J. Geophys. Res. 90*, 4756–4772.

Eckmann, J. P. and Ruelle, D. 1985. Ergodic theory of strange attractors. *Rev. Mod. Phys. 57*, 617–656.

Fahrbach, E., Brockmann, C. and Meincke, J. 1986. Horizontal mixing in the Atlantic equatorial undercurrent estimated from drifting buoy clusters. *J. Geophys. Res. 91*, 10557–10565.

Frisch, U. 1981. Fully developed turbulence and singularities. In: *Chaotic behaviour of deterministic systems* (eds. G. Iooss, H. G. Hellemann and R. Stora). Amsterdam: North Holland, 665–704.

Frisch, U. 1985. Fully developed turbulence and intermittency. In: *Turbulence and predictability in geophysical fluid dynamics and climate dynamics*. Proc. Int. School of Physics "Enrico Fermi," Course LXXXVIII (eds. M. Ghil, R. Benzi and G. Parisi). Amsterdam: North Holland, 71–88.

Frisch, U. and Morf, R. 1981. Intermittency in nonlinear dynamics and singularities at complex times. *Phys. Rev. A23*, 2673–2705.

Frisch, U. and Parisi, G. 1985. On the singularity structure of fully developed turbulence. In: *Turbulence and predictability in geophysical fluid dynamics and climate dynamics*. Proc. Int. School of Physics "Enrico Fermi," Course LXXXVIII (eds. M. Ghil, R. Benzi and G. Parisi). Amsterdam: North Holland, 84–88.

Frisch, U., Sulem, P. L. and Nelkin, M. 1978. A simple dynamical model of intermittent fully developed turbulence. *J. Fluid Mech. 87*, 719–736.

Grassberger, P. and Procaccia, I. 1983. Measuring the strangeness of strange attractors. *Physica 9D*, 189–208.

Halsey, T. C., Jensen, M. H., Kadanoff, L. P., Procaccia, I. and Shraiman, B. I. 1986. Fractal measures and their singularities: The characterization of strange sets. *Phys. Rev. A33*, 1141–1151.

Hofmann, E. E. 1985. The large-scale horizontal structure of the Antarctic circumpolar current from FGGE drifters. *J. Geophys. Res. 90*, 7087–7097.

Kirwan, A. D., Jr., McNally, G. J., Reyna, E. and Merrell, W. J., Jr. 1978. The near-surface circulation of the eastern North Pacific. *J. Phys. Ocean. 8*, 937–945.

Kirwan, A. D., Jr., McNally, G. J. and Pazan, S. 1978. Wind drag and relative separations of undrogued drifters. *J. Phys. Ocean. 8*, 1146–1150.

Kirwan, A. D., Jr., McNally, G. J., Pazan, S. and Wert, R. 1979. Analysis of surface current response to wind. *J. Phys. Ocean. 9*, 401–412.

Kirwan, A. D., Jr. and Cresswell, G. R. 1982. Observations of large and mesoscale motions in the near surface layer. In: *Topics in ocean physics*. Proc. Int. School of Physics "Enrico Fermi," Course LXXX

(eds. A. R. Osborne and P. Malanottee Rizzoli). Amsterdam: North Holland, 79–125.

Krauss, W., Dengg, J. and Hinrichsen, H.-H. 1989. The response of drifting buoys to currents and winds. *J. Geophys. Res. 94*, 3201–3210.

Large, W. J. and Van Loon, H. 1989. Large scale, low frequency variability of the 1979 FGGE surface buoy drifts and winds over the southern hemisphere. *J. Phys. Ocean. 19*, 216–232.

Lovejoy, S. 1982. The area-perimeter relationship for rain and cloud areas. *Science 216*, 185–187.

Lovejoy, S. and Mandelbrot, B. B. 1985. Fractal properties of rain, and a fractal model. *Tellus 37A*, 209–232.

Lovejoy S., Schertzer, D. and Tsonis, A. A. 1987. Functional boxcounting and multiple elliptical dimensions in rain. *Science 235*, 1036–1038.

Mandelbrot, B. B. 1967. How long is the coast of Britain? Statistical self-similarity and fractional dimension. *Science 155*, 636–638.

Mandelbrot, B. B. 1972. Possible refinement of the lognormal hypothesis concerning the distribution of energy dissipation in intermittent turbulence. In: *Statistical models and turbulence* (eds. M. Rosenblatt and C. Van Atta). Berlin: Springer Verlag, 333–351.

Mandelbrot, B. B. 1974. Intermittent turbulence in self-similar cascades: divergence of high moments and dimension of the carrier. *J. Fluid Mech. 62*, 331–358.

Mandelbrot, B. B. 1975. On the geometry of homogeneous turbulence, with stress on the fractal dimension of the iso-surfaces of scalars. *J. Fluid Mech. 72*, 401–416.

Mandelbrot, B. B. 1977. *Fractals: form, chance and dimension*. San Francisco: Freeman.

Mandelbrot, B. B. 1982. *The fractal geometry of nature*. San Francisco: Freeman.

McNally, G. J. 1981. Satellite-tracked drift buoy observations of the near-surface flow in the eastern mid-latitude North Pacific. *J. Geophys. Res. 86*, 8022–8030.

McNally, G. J., Patzert, W. C., Kirwan, A. D., Jr. and Vastano, A. C. 1983. The near-surface circulation of the North Pacific using satellite tracked drifting buoys. *J. Geophys. Res. 88*, 7507–7518.

McNally, G. J. and White, W. B. 1985. Wind driven flow in the mixed layer observed by drifting buoys during autumn–winter in the midlatitude North Pacific. *J. Phys. Ocean. 15*, 684–694.

Meneveau, C. and Sreenivasan, K. R. 1987. The multifractal spectrum of the dissipation field in turbulent flows. In: *Chaos '87* (ed. M. Duong-Van). *Nucl. Phys. B (Proc. Suppl.) 2*, 49–76.

Molinari, R. L., Spillane, M., Brooks, I., Atwood, D. and Duckett, C. 1981. Surface currents in the Caribbean Sea as deduced from Lagrangian observations. *J. Geophys. Res. 86*, 6537–6542.

Osborne, A. R., Kirwan, A. D., Jr., Provenzale, A. and Bergamasco, L. 1986. A search for chaotic behaviour in large and mesoscale motions in the Pacific Ocean. *Physica 23D*, 75–83.

Osborne, A. R. and Provenzale, A. 1989. Finite correlation dimension for stochastic processes with power law spectra. *Physica D*, in press.

Owens, W. B. 1984. A synoptic and statistical description of the Gulf Stream and subtropical gyre using SOFAR floats. *J. Phys. Ocean. 14*, 104–113.

Paladin, G. and Vulpiani, A. 1987. Anomalous scaling laws in multifractal objects. *Phys. Reports 156*, 147–225.

Panchev, S. 1971. *Random functions and turbulence*. Oxford: Pergamon.

Peterson, R. G. 1985. Drifter trajectories through a current meter array at Drake Passage. *J. Geophys. Res. 90*, 4883–4893.

Pietronero, L. and Tosatti, E. 1986. *Fractals in physics*. Amsterdam: North Holland.

Rhines, P. B. 1979. Geostrophic turbulence. *Ann. Rev. Fluid Mech. 11*, 401–441.

Richardson, P. L. 1983. Eddy kinetic energy in the North Atlantic from surface drifters. *J. Geophys. Res. 88*, 4355–4367.

Royer, T. C. and Emery, W. J. 1984. Circulation in the Bering Sea, 1982–82, based on satellite-tracked drifter observations. *J. Phys. Ocean. 14*, 1914–1920.

Salmon, R. 1982. Geostrophic turbulence. In: *Topics in ocean physics*. Proc. Int. School of Physics "Enrico Fermi," Course LXXX (eds. A. R. Osborne and P. Malanotte Rizzoli). Amsterdam: North Holland, 30–78.

Schertzer, D. and Lovejoy, S. 1983. Elliptical turbulence in the atmosphere. *Proceedings of the 4th Symposium on Turbulent Shear Flows*, 1–11 Nov. Karlsruhe: University of Karlsruhe Press.

Schertzer, D. and Lovejoy, S. 1987. Physical modeling and analysis of rain and clouds by anisotropic scaling multiplicative processes. *J. Geophys. Res. 92*, 9693–9714.

Schmitz, W. J., Jr., Price, J. F., Richardson, P. L., Owens, W. B. and Webb, D. C. 1981. A preliminary exploration of the Gulf Stream system with SOFAR floats. *J. Phys. Ocean. 11*, 1194–1204.

Schmitz, W. J., Jr. 1982. Abyssal eddy energy levels in the western North Pacific. *J. Phys. Ocean. 14*, 198–201.

Schmitz, W. J., Jr., Niiler, P. P., Bernstein, R. L. and Holland, W. R. 1982. Recent long-term mooring and instrument observation in the western North Pacific. *J. Geophys. Res. 87*, 9425–9440.

Shaw, P.-T. and Rossby, H. T. 1984. Towards a Lagrangian description of the Gulf Stream. *J. Phys. Ocean. 14*, 528–540.

Sreenivasan, K. R. and Meneveau, C. 1986. The fractal facets of turbulence. *J. Fluid Mech. 173*, 357–386.

Vastano, A. C., Hagan, D. E. and McNally, G. J. 1985. Lagrangian observation of surface circulation at the Emperor Seamount Chain. *J. Geophys. Res. 90*, 3325–3331.